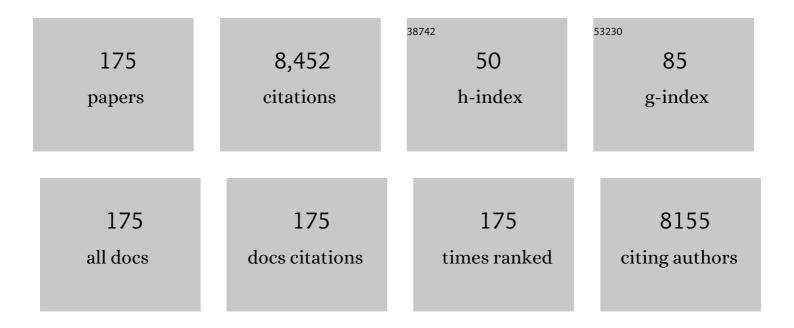
List of Publications by Year in descending order

Source: https://exaly.com/author-pdf/8792605/publications.pdf Version: 2024-02-01



#	Article	IF	CITATIONS
1	Defectâ€Rich Heterogeneous MoS ₂ /NiS ₂ Nanosheets Electrocatalysts for Efficient Overall Water Splitting. Advanced Science, 2019, 6, 1900246.	11.2	468
2	Hierarchical NiCo-LDH@NiOOH core-shell heterostructure on carbon fiber cloth as battery-like electrode for supercapacitor. Journal of Power Sources, 2018, 378, 248-254.	7.8	349
3	Enhancing Catalytic Activity of Titanium Oxide in Lithium–Sulfur Batteries by Band Engineering. Advanced Energy Materials, 2019, 9, 1900953.	19.5	326
4	Hierarchical CuCo2S4@NiMn-layered double hydroxide core-shell hybrid arrays as electrodes for supercapacitors. Chemical Engineering Journal, 2018, 336, 562-569.	12.7	236
5	Hierarchical NiCo-LDH/NiCoP@NiMn-LDH hybrid electrodes on carbon cloth for excellent supercapacitors. Journal of Materials Chemistry A, 2018, 6, 15040-15046.	10.3	233
6	Activating and optimizing the activity of NiCoP nanosheets for electrocatalytic alkaline water splitting through the V doping effect enhanced by P vacancies. Journal of Materials Chemistry A, 2019, 7, 24486-24492.	10.3	227
7	Heterostructural Graphene Quantum Dot/MnO ₂ Nanosheets toward Highâ€Potential Window Electrodes for Highâ€Performance Supercapacitors. Advanced Science, 2018, 5, 1700887.	11.2	215
8	Interlaced Ni-Co LDH nanosheets wrapped Co9S8 nanotube with hierarchical structure toward high performance supercapacitors. Chemical Engineering Journal, 2018, 351, 348-355.	12.7	197
9	Simultaneously Realizing Rapid Electron Transfer and Mass Transport in Jellyfishâ€Like Mott–Schottky Nanoreactors for Oxygen Reduction Reaction. Advanced Functional Materials, 2020, 30, 1910482.	14.9	173
10	Core-branched CoSe ₂ /Ni _{0.85} Se nanotube arrays on Ni foam with remarkable electrochemical performance for hybrid supercapacitors. Journal of Materials Chemistry A, 2018, 6, 19151-19158.	10.3	171
11	Atomic scale insights into structure instability and decomposition pathway of methylammonium lead iodide perovskite. Nature Communications, 2018, 9, 4807.	12.8	161
12	Nanoarchitectured Design of Vertical‣tanding Arrays for Supercapacitors: Progress, Challenges, and Perspectives. Advanced Functional Materials, 2021, 31, 2006030.	14.9	150
13	Bamboo-like amorphous carbon nanotubes clad in ultrathin nickel oxide nanosheets for lithium-ion battery electrodes with long cycle life. Carbon, 2015, 84, 491-499.	10.3	145
14	Field Emission from a Composite of Graphene Sheets and ZnO Nanowires. Journal of Physical Chemistry C, 2009, 113, 9164-9168.	3.1	127
15	Bifunctional Electrocatalysts Based on Mo-Doped NiCoP Nanosheet Arrays for Overall Water Splitting. Nano-Micro Letters, 2019, 11, 55.	27.0	125
16	A composite solid polymer electrolyte incorporating MnO ₂ nanosheets with reinforced mechanical properties and electrochemical stability for lithium metal batteries. Journal of Materials Chemistry A, 2020, 8, 2021-2032.	10.3	118
17	In Situ Synthesis of Vertical Standing Nanosized NiO Encapsulated in Graphene as Electrodes for Highâ€Performance Supercapacitors. Advanced Science, 2018, 5, 1700687.	11.2	117
18	Rational constructing free-standing Se doped nickel-cobalt sulfides nanotubes as battery-type electrode for high-performance supercapattery. Journal of Power Sources, 2018, 407, 6-13.	7.8	110

#	Article	IF	CITATIONS
19	<i>In situ</i> encapsulated Fe ₃ O ₄ nanosheet arrays with graphene layers as an anode for high-performance asymmetric supercapacitors. Journal of Materials Chemistry A, 2017, 5, 24594-24601.	10.3	105
20	Designing oxygen bonding between reduced graphene oxide and multishelled Mn ₃ O ₄ hollow spheres for enhanced performance of supercapacitors. Journal of Materials Chemistry A, 2019, 7, 6686-6694.	10.3	103
21	Rational construction of nickel cobalt sulfide nanoflakes on CoO nanosheets with the help of carbon layer as the battery-like electrode for supercapacitors. Journal of Power Sources, 2017, 362, 64-72.	7.8	99
22	Flexible and Highâ€Loading Lithium–Sulfur Batteries Enabled by Integrated Threeâ€Inâ€One Fibrous Membranes. Advanced Energy Materials, 2019, 9, 1902001.	19.5	98
23	Few-layer MoS ₂ anchored at nitrogen-doped carbon ribbons for sodium-ion battery anodes with high rate performance. Journal of Materials Chemistry A, 2017, 5, 17963-17972.	10.3	93
24	Crystalline molybdenum carbideâ^'amorphous molybdenum oxide heterostructures: In situ surface reconfiguration and electronic states modulation for Liâ^'S batteries. Energy Storage Materials, 2022, 47, 345-353.	18.0	92
25	Three-dimensional graphene-reinforced Cu foam interlayer for brazing C/C composites and Nb. Carbon, 2017, 118, 723-730.	10.3	88
26	Modification strategies on transition metal-based electrocatalysts for efficient water splitting. Journal of Energy Chemistry, 2021, 58, 446-462.	12.9	88
27	Partial sulfuration-induced defect and interface tailoring on bismuth oxide for promoting electrocatalytic CO ₂ reduction. Journal of Materials Chemistry A, 2020, 8, 2472-2480.	10.3	82
28	Controlled synthesis of MOF-derived quadruple-shelled CoS2 hollow dodecahedrons as enhanced electrodes for supercapacitors. Electrochimica Acta, 2019, 312, 54-61.	5.2	81
29	Corrosion behavior of stainless steel-tungsten carbide joints brazed with AgCuX (XÂ=ÂIn, Ti) alloys. Corrosion Science, 2022, 200, 110231.	6.6	80
30	Blowing Iron Chalcogenides into Two-Dimensional Flaky Hybrids with Superior Cyclability and Rate Capability for Potassium-Ion Batteries. ACS Nano, 2021, 15, 2506-2519.	14.6	79
31	P-Doped NiCo ₂ S ₄ nanotubes as battery-type electrodes for high-performance asymmetric supercapacitors. Dalton Transactions, 2018, 47, 8771-8778.	3.3	75
32	Relatively low temperature synthesis of graphene by radio frequency plasma enhanced chemical vapor deposition. Applied Surface Science, 2011, 257, 6531-6534.	6.1	73
33	Vertically oriented few-layer graphene-nanocup hybrid structured electrodes for high-performance supercapacitors. Journal of Materials Chemistry A, 2015, 3, 12396-12403.	10.3	73
34	Oxygen-vacancy-rich nickel-cobalt layered double hydroxide electrode for high-performance supercapacitors. Journal of Colloid and Interface Science, 2019, 554, 59-65.	9.4	70
35	Designing and constructing core-shell NiCo2S4@Ni3S2 on Ni foam by facile one-step strategy as advanced battery-type electrodes for supercapattery. Journal of Colloid and Interface Science, 2019, 536, 456-462.	9.4	70
36	Ar plasma treatment on few layer graphene sheets for enhancing their field emission properties. Journal Physics D: Applied Physics, 2010, 43, 055302.	2.8	69

#	Article	IF	CITATIONS
37	Controllable synthesis of core-branch Ni3S2/Co9S8 directly on nickel foam as an efficient bifunctional electrocatalyst for overall water splitting. Journal of Power Sources, 2018, 401, 329-335.	7.8	69
38	Dense Crystalline–Amorphous Interfacial Sites for Enhanced Electrocatalytic Oxygen Evolution. Advanced Functional Materials, 2022, 32, 2107056.	14.9	69
39	Iron Selenide Microcapsules as Universal Conversionâ€Typed Anodes for Alkali Metalâ€Ion Batteries. Small, 2021, 17, e2005745.	10.0	66
40	Mesostructured Carbon Nanotube-on-MnO ₂ Nanosheet Composite for High-Performance Supercapacitors. ACS Applied Materials & Interfaces, 2018, 10, 38963-38969.	8.0	65
41	A high-performance supercapacitor of vertically-oriented few-layered graphene with high-density defects. Nanoscale, 2015, 7, 3675-3682.	5.6	63
42	Microstructures and tensile behavior of carbon nanotubes reinforced Cu matrix composites with molecular-level dispersion. Materials & Design, 2012, 34, 298-301.	5.1	60
43	Field Emission Properties of Hybrid Carbon Nanotubeâ^'ZnO Nanoparticles. Journal of Physical Chemistry C, 2008, 112, 17702-17708.	3.1	58
44	S doped NiCo2O4 nanosheet arrays by Ar plasma: An efficient and bifunctional electrode for overall water splitting. Journal of Colloid and Interface Science, 2020, 560, 34-39.	9.4	57
45	Sandwich-like structured NiSe2/Ni2P@FeP interface nanosheets with rich defects for efficient electrocatalytic water splitting. Journal of Power Sources, 2020, 445, 227294.	7.8	56
46	Hierarchical CuCo ₂ O ₄ @NiMoO ₄ core–shell hybrid arrays as a battery-like electrode for supercapacitors. Inorganic Chemistry Frontiers, 2017, 4, 1575-1581.	6.0	55
47	Interlayer design to control interfacial microstructure and improve mechanical properties of active brazed Invar/SiO2–BN joint. Materials Science & Engineering A: Structural Materials: Properties, Microstructure and Processing, 2013, 575, 199-205.	5.6	54
48	Nanosized core–shell structured graphene–MnO ₂ nanosheet arrays as stable electrodes for superior supercapacitors. Journal of Materials Chemistry A, 2017, 5, 10678-10686.	10.3	54
49	Highly conductive Mn3O4/MnS heterostructures building multi-shelled hollow microspheres for high-performance supercapacitors. Chemical Engineering Journal, 2020, 392, 123890.	12.7	54
50	Low resistance VFG-Microporous hybrid Al-based electrodes for supercapacitors. Nano Energy, 2016, 26, 657-667.	16.0	52
51	A CoMoO ₄ –Co ₂ Mo ₃ O ₈ heterostructure with valence-rich molybdenum for a high-performance hydrogen evolution reaction in alkaline solution. Journal of Materials Chemistry A, 2019, 7, 16761-16769.	10.3	50
52	Free-standing porous Ni2P-Ni5P4 heterostructured arrays for efficient electrocatalytic water splitting. Journal of Colloid and Interface Science, 2019, 552, 332-336.	9.4	49
53	W doping dominated NiO/NiS2 interfaced nanosheets for highly efficient overall water splitting. Journal of Colloid and Interface Science, 2020, 562, 363-369.	9.4	47
54	Fe doped Ni ₅ P ₄ nanosheet arrays with rich P vacancies <i>via</i> phase transformation for efficient overall water splitting. Nanoscale, 2020, 12, 6204-6210.	5.6	47

#	Article	IF	CITATIONS
55	Engineering Se vacancies to promote the intrinsic activities of P doped NiSe2 nanosheets for overall water splitting. Journal of Colloid and Interface Science, 2020, 571, 260-266.	9.4	47
56	Control interfacial microstructure and improve mechanical properties of TC4-SiO2f/SiO2 joint by AgCuTi with Cu foam as interlayer. Ceramics International, 2016, 42, 16619-16625.	4.8	46
57	Modifying the electrochemical performance of vertically-oriented few-layered graphene through rotary plasma processing. Journal of Materials Chemistry A, 2018, 6, 908-917.	10.3	46
58	Welding and Joining of Titanium Aluminides. Materials, 2014, 7, 4930-4962.	2.9	45
59	Hierarchical Fe2O3 and NiO nanotube arrays as advanced anode and cathode electrodes for high-performance asymmetric supercapacitors. Journal of Alloys and Compounds, 2019, 794, 255-260.	5.5	45
60	Au nanoparticle-decorated NiCo2O4 nanoflower with enhanced electrocatalytic activity toward methanol oxidation. Journal of Alloys and Compounds, 2018, 732, 460-469.	5.5	44
61	Pre-infiltration and brazing behaviors of Cf/C composites with high temperature Ti Si eutectic alloy. Carbon, 2018, 140, 57-67.	10.3	43
62	Rich P vacancies modulate Ni2P/Cu3P interfaced nanosheets for electrocatalytic alkaline water splitting. Journal of Colloid and Interface Science, 2020, 564, 37-42.	9.4	43
63	Atomic structure and migration dynamics of MoS2/LixMoS2 interface. Nano Energy, 2018, 48, 560-568.	16.0	42
64	Brazing ZTA ceramic to TC4 alloy using the Cu foam as interlayer. Vacuum, 2018, 155, 7-15.	3.5	42
65	Characterization of Al/Ni multilayers and their application in diffusion bonding of TiAl to TiC cermet. Thin Solid Films, 2012, 520, 3528-3531.	1.8	41
66	Promoting Bifunctional Water Splitting by Modification of the Electronic Structure at the Interface of NiFe Layered Double Hydroxide and Ag. ACS Applied Materials & Interfaces, 2021, 13, 26055-26063.	8.0	41
67	Origin of low dielectric loss and giant dielectric response in (Nb+Al) coâ€doped strontium titanate. Journal of the American Ceramic Society, 2018, 101, 5089-5097.	3.8	40
68	Exploring CoP core–shell nanosheets by Fe and Zn dual cation doping as efficient electrocatalysts for overall water splitting. Catalysis Science and Technology, 2020, 10, 1395-1400.	4.1	40
69	Ultrathin NiFe-layered double hydroxide decorated NiCo2O4 arrays with enhanced performance for supercapacitors. Applied Surface Science, 2019, 465, 929-936.	6.1	38
70	In-Situ synthesized TiC nano-flakes reinforced C/C composite-Nb brazed joint. Journal of the European Ceramic Society, 2018, 38, 1059-1068.	5.7	37
71	Amorphous Iron(III)â€Borate Nanolattices as Multifunctional Electrodes for Selfâ€Đriven Overall Water Splitting and Rechargeable Zinc–Air Battery. Small, 2018, 14, e1802829.	10.0	37
72	Rational construction of core–shell Ni3S2@Ni(OH)2 nanostructures as battery-like electrodes for supercapacitors. Inorganic Chemistry Frontiers, 2018, 5, 1985-1991.	6.0	37

#	Article	IF	CITATIONS
73	Microwave-assisted fast synthesis of hierarchical NiCo ₂ O ₄ nanoflower-like supported Ni(OH) ₂ nanoparticles with an enhanced electrocatalytic activity towards methanol oxidation. Inorganic Chemistry Frontiers, 2018, 5, 172-182.	6.0	36
74	C/SiC composite-Ti6Al4V joints brazed with negative thermal expansion ZrP2WO12 nanoparticle reinforced AgCu alloy. Journal of the European Ceramic Society, 2019, 39, 755-761.	5.7	36
75	Combustion synthesis of TiAl intermetallics and their simultaneous joining to carbon/carbon composites. Scripta Materialia, 2011, 65, 261-264.	5.2	35
76	Designed formation of NiO@C@Cu2O hybrid arrays as battery-like electrode with enhanced electrochemical performances. Ceramics International, 2017, 43, 15410-15417.	4.8	35
77	Origin of high dielectric permittivity and low dielectric loss of Sr0.985Ce0.01TiO3 ceramics under different sintering atmospheres. Journal of Alloys and Compounds, 2019, 782, 51-58.	5.5	35
78	In situ synthesis of core-shell vanadium nitride@N-doped carbon microsheet sponges as high-performance anode materials for solid-state supercapacitors. Journal of Colloid and Interface Science, 2020, 560, 122-129.	9.4	34
79	A free-standing manganese cobalt sulfide@cobalt nickel layered double hydroxide core–shell heterostructure for an asymmetric supercapacitor. Dalton Transactions, 2020, 49, 196-202.	3.3	34
80	Optimize the electrocatalytic performances of NiCoP for water splitting by the synergic effect of S dopant and P vacancy. International Journal of Hydrogen Energy, 2020, 45, 16161-16168.	7.1	34
81	Combustion joining of carbon–carbon composites to TiAl intermetallics using a Ti–Al–C powder composite interlayer. Composites Science and Technology, 2015, 115, 72-79.	7.8	33
82	Cerium doped strontium titanate with stable high permittivity and low dielectric loss. Journal of Alloys and Compounds, 2019, 772, 1105-1112.	5.5	33
83	Processing, microstructure and mechanical properties of vacuum-brazed Al2O3/Ti6Al4V joints. Materials Science & Engineering A: Structural Materials: Properties, Microstructure and Processing, 2012, 535, 62-67.	5.6	32
84	Wetting and brazing of Cf/C composites with Si–Zr eutectic alloys: The formation of nano- and coarse-SiC reaction layers. Carbon, 2020, 167, 92-103.	10.3	31
85	Graphene-enhanced Cu composite interlayer for contact reaction brazing aluminum alloy 6061. Vacuum, 2017, 136, 142-145.	3.5	30
86	Emerging elemental two-dimensional materials for energy applications. Journal of Materials Chemistry A, 2021, 9, 18793-18817.	10.3	30
87	Regulating the interfacial reaction of Sc2W3O12/AgCuTi composite filler by introducing a carbon barrier layer. Carbon, 2022, 191, 290-300.	10.3	30
88	Interfacial microstructure and mechanical properties of SiC joints achieved by reactive air brazing using Ag-V2O5 filler. Journal of the European Ceramic Society, 2019, 39, 2617-2625.	5.7	28
89	Ultra-lightweight ion-sieving membranes for high-rate lithium sulfur batteries. Chemical Engineering Journal, 2022, 430, 132698.	12.7	28
90	A fast micro–nano liquid layer induced construction of scaled-up oxyhydroxide based electrocatalysts for alkaline water splitting. Journal of Materials Chemistry A, 2021, 9, 26777-26787.	10.3	27

#	Article	IF	CITATIONS
91	Mn and S dual-doping of MOF-derived Co3O4 electrode array increases the efficiency of electrocatalytic generation of oxygen. Journal of Colloid and Interface Science, 2019, 557, 28-33.	9.4	26
92	Carbon nanotubes-reinforced Ni foam interlayer for brazing SiO2-BN with Ti6Al4V alloy using TiZrNiCu brazing alloy. Ceramics International, 2018, 44, 3684-3691.	4.8	24
93	Joining of SiO ₂ –BN ceramic to Nb using a CNT-reinforced brazing alloy. RSC Advances, 2014, 4, 64238-64243.	3.6	23
94	Fabrication of 3D Ni nanosheet array on Crofer22APU interconnect and NiO-YSZ anode support to sinter with small-size Ag nanoparticles for low-temperature sealing SOFCs. International Journal of Hydrogen Energy, 2018, 43, 2977-2989.	7.1	23
95	"One-for-All―strategy to design oxygen-deficient triple-shelled MnO ₂ and hollow Fe ₂ O ₃ microcubes for high energy density asymmetric supercapacitors. Dalton Transactions, 2019, 48, 8623-8632.	3.3	23
96	Brazing YSZ ceramics by a novel SiO2 nanoparticles modified Ag filler. Ceramics International, 2020, 46, 16493-16501.	4.8	23
97	Root-like C/SiC surface structure fabricated by the thermal and electrochemical corrosion for brazing to Nb. Composites Part B: Engineering, 2021, 218, 108942.	12.0	22
98	All-in-One Sulfur Host: Smart Controls of Architecture and Composition for Accelerated Liquid–Solid Redox Conversion in Lithium–Sulfur Batteries. ACS Applied Materials & Interfaces, 2021, 13, 39424-39434.	8.0	22
99	Synthesis of graphene on a Ni film by radio-frequency plasma-enhanced chemical vapor deposition. Science Bulletin, 2012, 57, 3040-3044.	1.7	21
100	In situ consume excessive Ti element and form fine Ti based compounds as reinforcements for strengthening C/C-TC4 joints. Vacuum, 2017, 143, 303-311.	3.5	21
101	Spontaneously Formed Mottâ€Schottky Electrocatalyst for Lithiumâ€Sulfur Batteries. Advanced Materials Interfaces, 2020, 7, 1902092.	3.7	21
102	Plasma treatment on SiO2f/SiO2 composites for their assisted brazing with Nb. Vacuum, 2016, 123, 136-139.	3.5	20
103	Sea urchin-like CuCo ₂ S ₄ microspheres with a controllable interior structure as advanced electrode materials for high-performance supercapacitors. Inorganic Chemistry Frontiers, 2020, 7, 603-609.	6.0	20
104	MCo2O4 (M=Co, Mn, Ni, Zn) nanosheet arrays constructed by two-dimension metal-organic frameworks as binder-free electrodes for lithium-ion batteries. Vacuum, 2019, 169, 108959.	3.5	19
105	Self-Assembly Lightweight Honeycomb-Like Prussian Blue Analogue on Cu Foam for Lithium Metal Anode. ACS Applied Materials & Interfaces, 2021, 13, 23803-23810.	8.0	19
106	Brazing C/C composites to DD3 alloy with a novel Ag–Cr active braze. Ceramics International, 2022, 48, 15090-15097.	4.8	19
107	A general strategy to construct N-doped carbon-confined MoO2 and MnO for high-performance hybrid supercapacitors. Vacuum, 2019, 165, 179-185.	3.5	18
108	Characterization of hydrogenated niobium interlayer and its application in TiAl/Ti2AlNb diffusion bonding. International Journal of Hydrogen Energy, 2019, 44, 6929-6937.	7.1	18

#	Article	IF	CITATIONS
109	Microstructure and mechanical properties of the AlON / Ti6Al4V active element brazing joint. Materials Science & Engineering A: Structural Materials: Properties, Microstructure and Processing, 2020, 793, 139859.	5.6	18
110	Constructing MoS ₂ /CoMo ₂ S ₄ /Co ₃ S ₄ nanostructures supported by graphene layers as the anode for lithium-ion batteries. Dalton Transactions, 2020, 49, 1167-1172.	3.3	17
111	Realizing the air brazing of ZrO2 ceramics through Al metal. Journal of Materiomics, 2022, 8, 662-668.	5.7	17
112	Brazing SiO 2f /SiO 2 with TC4 alloy with the help of coating graphene. Vacuum, 2017, 145, 241-244.	3.5	16
113	Microstructure and mechanical properties of the SiC/Nb joint brazed using AgCuTi+B4C composite filler metal. International Journal of Refractory Metals and Hard Materials, 2019, 85, 105049.	3.8	16
114	Wetting of Si–14Ti alloy on SiCf/SiC and C/C composites and their brazed joint at high temperatures. Ceramics International, 2021, 47, 13845-13852.	4.8	16
115	Microstructure design of C/C composites through electrochemical corrosion for brazing to Nb. Journal of Materials Science and Technology, 2022, 104, 33-40.	10.7	16
116	Oxidation behavior of ferritic stainless steel interconnect coated by a simple diffusion bonded cobalt protective layer for solid oxide fuel cells. Corrosion Science, 2020, 172, 108739.	6.6	16
117	Releasing the residual stress of Cf/SiC-GH3536 joint by designing an Ag-Cu-TiÂ+ÂSc2(WO4)3 composite filler metal. Journal of Materials Science and Technology, 2022, 108, 102-109.	10.7	15
118	Non-destructive measurement of residual stress distribution as a function of depth in sapphire/Ti6Al4V brazing joint via Raman spectra. Ceramics International, 2019, 45, 3284-3289.	4.8	14
119	Interfacial reaction and brazing behaviour of SiCf/SiC with Cf/C composites using Si-10Zr alloy at high temperatures. Journal of the European Ceramic Society, 2021, 41, 1142-1150.	5.7	14
120	Interfacial microstructure and improved wetting mechanism of SiO 2f /SiO 2 brazed with Nb by plasma treatment. Vacuum, 2017, 143, 320-328.	3.5	13
121	Joining SiO2 based ceramics: recent progress and perspectives. Journal of Materials Science and Technology, 2022, 108, 110-124.	10.7	13
122	Vacuum brazing of AlON and Ti2AlNb with LiAlSiO4 enhanced Ag–Cu–Ti composite fillers: Microstructure, mechanical properties and measurement of residual stress. Materials Science & Engineering A: Structural Materials: Properties, Microstructure and Processing, 2022, 846, 143277.	5.6	13
123	Syntheses of carbon nanomaterials by radio frequency plasma enhanced chemical vapor deposition. Journal of Alloys and Compounds, 2009, 486, 265-272.	5.5	12
124	The crystal orientation relation and macroscopic surface roughness in hetero-epitaxial graphene grown on Cu/mica. Nanotechnology, 2014, 25, 185602.	2.6	12
125	Effects of oxygen on growth of carbon nanotubes prospered by PECVD. Materials Research Bulletin, 2014, 49, 66-70.	5.2	12
126	Regulating the surface structure of SiO 2f /SiO 2 composite for assisting in brazing with Nb. Materials Letters, 2016, 182, 159-162.	2.6	12

#	Article	IF	CITATIONS
127	Microstructure evolution and mechanical properties of Co coated AISI 441 ferritic stainless steel/ YSZ reactive air brazed joint. International Journal of Hydrogen Energy, 2021, 46, 8758-8766.	7.1	12
128	Effects of total CH4/Ar gas pressure on the structures and field electron emission properties of carbon nanomaterials grown by plasma-enhanced chemical vapor deposition. Applied Surface Science, 2009, 256, 1542-1547.	6.1	11
129	Antimony nanocrystals self-encapsulated within bio-oil derived carbon for ultra-stable sodium storage. Journal of Colloid and Interface Science, 2021, 582, 459-466.	9.4	11
130	Effect of catalyst film thickness on the structures of vertically-oriented few-layer graphene grown by PECVD. RSC Advances, 2014, 4, 44434-44441.	3.6	10
131	Plasma-induced surface reorganization of porous Co3O4-CoO heterostructured nanosheets for electrocatalytic water oxidation. Journal of Colloid and Interface Science, 2020, 565, 400-404.	9.4	10
132	Bioinspired Metal-Intermetallic Laminated Composites for the Fabrication of Superhydrophobic Surfaces with Responsive Wettability. ACS Applied Materials & Interfaces, 2021, 13, 5834-5843.	8.0	10
133	Stable lithium metal anode achieved by shortening diffusion path on solid electrolyte interface derived from Cu2O lithiophilic layer. Chemical Engineering Journal, 2022, 433, 133689.	12.7	10
134	Relieving residual stress in brazed joint between SiC and Nb using a 3D-SiO2-fiber ceramic interlayer. Vacuum, 2018, 149, 93-95.	3.5	9
135	Joining of yttria stabilised zirconia to Ti6Al4V alloy using novel CuO nanostructure reinforced Cu foam interlayer. Materials Letters, 2019, 253, 105-108.	2.6	9
136	Making Superhydrophobic Surfaces with Microstripe Array Structure by Diffusion Bonding and Their Applications in Magnetic Control Microdroplet Release Systems. Advanced Materials Interfaces, 2017, 4, 1700918.	3.7	8
137	Atomic-scale structural and chemical evolution of Li3V2(PO4)3 cathode cycled at high voltage window. Nano Research, 2019, 12, 1675-1681.	10.4	8
138	In situ TiSi2 microarray reinforced Si–Ti eutectic colonies in Cf/C composite joints for high-temperature application. Ceramics International, 2020, 46, 10495-10502.	4.8	8
139	Evolution and formation mechanism of the interfacial microstructure on diffusion bonded joints of single crystal Ni-based superalloys to Ti3AlC2 ceramic with Ni interlayer. Vacuum, 2021, 185, 110027.	3.5	8
140	Field emission properties of hybrid few-layer graphene-carbon nanotubes. Materials Research Express, 2014, 1, 025601.	1.6	7
141	Nano tungsten reinforced carbon cloth interlayer for brazing C/SiC composites to Nb. Journal of Manufacturing Processes, 2020, 58, 1270-1273.	5.9	7
142	Constructing NiS–VS heterostructured nanosheets for efficient overall water splitting. Inorganic Chemistry Frontiers, 2020, 7, 4924-4929.	6.0	7
143	β-LiAlSiO4 negative thermal expansion network interlayer for C/C–Nb brazing joint. Ceramics International, 2020, 46, 14232-14234.	4.8	7
144	Synthesis of a composite consisting of carbon nanotubes and graphite shell-encapsulated cobalt nanoparticles using plasma-enhanced chemical vapor deposition. Applied Surface Science, 2009, 256, 1486-1491.	6.1	6

#	Article	IF	CITATIONS
145	Controllable fabrication of carbon nanotubes on catalysts derived from PS-b-P2VP block copolymer template and in situ synthesis of carbon nanotubes/Au nanoparticles composite materials. Materials Chemistry and Physics, 2010, 119, 249-253.	4.0	6
146	The relation between residual stress, interfacial structure and the joint property in the SiO2f/SiO2-Nb joints. Scientific Reports, 2017, 7, 4187.	3.3	6
147	Understanding the Effect of Surface Machining on the YSZ/Ti6Al4V Joint via Image Based Modelling. Scientific Reports, 2019, 9, 12027.	3.3	6
148	Mechanical durable ceria superhydrophobic coating fabricated by simple hot-press sintering. Applied Surface Science, 2020, 529, 147113.	6.1	6
149	Surface synthesis of aluminum borate whiskers on the ZTA ceramics and its application to joining. Ceramics International, 2021, 47, 11269-11275.	4.8	6
150	Joining of Al2O3 to ZTA using a B2O3–Al2O3–SiO2 glass with in-situ precipitated whiskers. Ceramics International, 2021, 47, 25541-25550.	4.8	6
151	A novel brush surface structure of SiCf/SiC composites designed for brazing improvement. Vacuum, 2022, 195, 110700.	3.5	6
152	Design CuZr alloy to control Ti diffusion and reaction layer thickness in C/C-TC4 joins. Materials Characterization, 2022, , 111889.	4.4	6
153	Y2W3O12@SiO2 composite particles for regulating thermal expansion and interfacial reactions in BaZr0.1Ce0.7Y0.1Yb0.1O3-Î/AISI 441 joints. Composites Part B: Engineering, 2022, 242, 110108.	12.0	6
154	Lithium–Sulfur Batteries: Flexible and High‣oading Lithium–Sulfur Batteries Enabled by Integrated Threeâ€Inâ€One Fibrous Membranes (Adv. Energy Mater. 38/2019). Advanced Energy Materials, 2019, 9, 1970147.	19.5	5
155	Magnesiothermic reduction of SiO2f/SiO2 composites for brazing with Nb using AgCuTi. Journal of Manufacturing Processes, 2019, 46, 26-33.	5.9	5
156	The role of Al diffusion behavior in the process of forming a super-reliable Al2O3 protective layer during reactive air aluminization. Applied Surface Science, 2020, 518, 146242.	6.1	5
157	A low-temperature sealing method for metal-supported oxide fuel cell applications: Ni–Sn transient liquid phase bonding. Vacuum, 2021, 187, 110048.	3.5	5
158	Joining ZTA ceramics by using whiskers reinforced borosilicate glasses for high-temperature applications. Materials Letters, 2021, 304, 130583.	2.6	5
159	Brazing ZTA ceramic and Ti6Al4V alloy directly in air: Excellent oxidation resistance at 800°C. Ceramics International, 2022, 48, 9631-9639.	4.8	5
160	Confirming the key role of Ar ⁺ ion bombardment in the growth feature of nanostructured carbon materials by PECVD. Nanotechnology, 2017, 28, 475601.	2.6	4
161	A Highly Efficient Electrocatalyst Derived from Polyaniline@CNTsâ^'SPS for the Oxygen Reduction Reaction. ChemElectroChem, 2018, 5, 195-200.	3.4	4
162	The normal spectral emittance of the real surface from worked aero-engine nozzle. Applied Thermal Engineering, 2019, 150, 641-650.	6.0	4

#	Article	IF	CITATIONS
163	Microstructure evolution and mechanical properties of SiO2f/SiO2 composites joints brazed by bismuth glass. Ceramics International, 2021, 48, 5840-5840.	4.8	4
164	Corrosion behavior of Ag-based alloy in simulated body fluid solution. Vacuum, 2022, 197, 110850.	3.5	4
165	Mottâ€Schottky Electrocatalyst: Spontaneously Formed Mottâ€Schottky Electrocatalyst for Lithiumâ€Sulfur Batteries (Adv. Mater. Interfaces 22/2020). Advanced Materials Interfaces, 2020, 7, 2070122.	3.7	3
166	Silver particle interlayer with high dislocation density for improving the joining of BaZr0.1Ce0.7Y0.1Yb0.1O3- electrolyte and AISI 441 interconnect. Journal of Materiomics, 2022, 8, 1001-1008.	5.7	3
167	SiO2 migration mechanism at the joints of SiO2f/SiO2 composite brazed by bismuth glass. Ceramics International, 2022, 48, 24319-24325.	4.8	3
168	Patterned Carbon Nanotubes Fabricated by the Combination of Microcontact Printing and Diblock Copolymer Micelles. Journal of Nanoscience and Nanotechnology, 2010, 10, 508-513.	0.9	2
169	Joining Alumina and Sapphire by Growing Aluminium Borate Whiskers In-Situ, and the Whiskers' Orientation Relationship with the Sapphire Substrate. Materials, 2020, 13, 175.	2.9	2
170	Joining silicon nitride ceramics in air by pure aluminum filler. Ceramics International, 2021, 47, 17794-17798.	4.8	2
171	Microstructure and mechanical properties of Al ₂ O ₃ ceramic joints achieved by Agâ€siO ₂ braze in air. International Journal of Applied Ceramic Technology, 2022, 19, 508-513.	2.1	2
172	A study of mechanical property and corrosion resistance of modified silica glass. Vacuum, 2022, 203, 111233.	3.5	2
173	Effect of Ni concentration on solderability, microstructure and hardness of SAC0705-xNi solder joints on Cu and graphene-coated Cu substrates. Modern Physics Letters B, 2019, 33, 1850425.	1.9	1
174	Rechargeable Zinc–Air Batteries: Amorphous Iron(III)â€Borate Nanolattices as Multifunctional Electrodes for Selfâ€Driven Overall Water Splitting and Rechargeable Zinc–Air Battery (Small 48/2018). Small, 2018, 14, 1870233.	10.0	0
175	Introduction to water splitting technologies. , 2022, , 3-24.		0